BIOCHEMISTRY

Two ligand-binding sites in CO-reducing V nitrogenase reveal a general mechanistic principle

Michael Rohde[1], Konstantin Laun[2], Ingo Zebger[2], Sven T. Stripp[3], Oliver Einsle[1]*

Besides its role in biological nitrogen fixation, vanadium-containing nitrogenase also reduces carbon monoxide (CO) to hydrocarbons, in analogy to the industrial Fischer-Tropsch process. The protein yields 93% of ethylene (C_2H_4), implying a C–C coupling step that mandates the simultaneous binding of two CO at the active site FeV cofactor. Spectroscopic data indicated multiple CO binding events, but structural analyses of Mo and V nitrogenase only confirmed a single site. Here, we report the structure of a two CO-bound state of V nitrogenase at 1.05 Å resolution, with one μ-bridging and one terminal CO molecule. This additional, specific ligand binding site suggests a mechanistic route for CO reduction and hydrocarbon formation, as well as a second access pathway for protons required during the reaction. Moreover, carbonyls are strong-field ligands that are chemically similar to mechanistically relevant hydrides that may be formed and used in a fully analogous fashion.

INTRODUCTION

As the only known enzymes able to reduce atmospheric N_2, nitrogenases are key to providing bioavailable nitrogen to the entire biosphere (*1*, *2*). They catalyze the biological equivalent to the industrial Haber-Bosch process at ambient conditions, using low-potential electrons and adenosine 5′-triphosphate (ATP). Nitrogenases are a family of three related metalloenzymes whose most prominent difference lies in their unique active site cofactor (*3*, *4*). The best-studied class of nitrogenases uses molybdenum in a [Mo:7Fe:9S:C]:homocitrate cluster, the FeMo cofactor (Fig. 1A and fig. S1) (*5*). Under conditions of low Mo availability, many diazotrophs activate an alternative set of genes encoding a vanadium-dependent enzyme, whose FeV cofactor is a [V:7Fe:8S:C:CO_3^{2-}]:homocitrate moiety that not only exchanges the heterometal but also has one of the μ$_2$-bridging sulfide ligands at its belt replaced for carbonate (Fig. 1B) (*6*). Although there is no structural data available for the third class of nitrogenases that dispenses of any metal other than iron, an FeFe cofactor with a core composition of [8Fe:9S:C] is commonly assumed (*7*, *8*). Many mechanistic aspects of nitrogenase catalysis remain under debate, but a consensus has emerged that the active site cofactor successively accumulates four electrons in the form of bridging hydrides at the cluster surface (*3*, *9*, *10*). The reductive elimination of H_2, at the cost of two of these electrons, then leaves the cluster in a super-reduced state that activates and reduces the inert N_2 (*11*). All types of nitrogenases follow the same mechanistic path and reductively eliminate H_2 for N_2 activation (*12*). Fe and V nitrogenases were long seen as backup systems to sustain diazotrophic microorganisms under heterometal limitation. The discovery that CO, a noncompetitive inhibitor for all substrates other than protons (*13*), is also a substrate for V nitrogenase but not its Mo-containing relative was therefore of high interest for enzymology and biotechnological applications, e.g., in biofuel production (*14*). Similar to the physiological fixation of N_2, the reduction of CO to hydrocarbons also has its equivalence in industrial chemistry, in the form of the 1925 Fischer-Tropsch

process (*15*). In both cases, the reactant CO is not fully reduced to methane but shows a propensity for C-C bond formation resulting in a spectrum of products. V nitrogenase yields ethylene, C_2H_4, as a main product of CO reduction (>93%), with minor amounts of ethane, propane, and methane (*16*). In contrast to the Fischer-Tropsch reaction, no hydroxides, aldehydes, or carboxylates were reported, implying that oxygen atoms are quantitatively released as H_2O.

The site and mode of substrate binding to nitrogenase cofactors has long been a matter of speculation, as the enzyme is isolated in a resting state where all metal centers of the cofactor seem coordinatively saturated (Fig. 1, A and B) (*5*). Various binding modes for N_2 were suggested, with an overall preference either for a side-on association with one of the four Fe faces of the cofactor or an end-on binding to one of the six iron ions that form a trigonal prism around the central carbide of the cluster. In these tetrahedral sites, the Fe ion is closer to the plane formed by three sulfide ligands than to the fourth ligand, the central carbide (*17*). Inspired by this arrangement, Peters and co-workers (*18*, *19*) generated a series of tris-phosphine compounds with an axial binding of N_2, resulting in trigonally bipyramidal complexes that stabilized low-valent iron. They varied the proximal axial ligand—initially boron—also to carbon and reported catalytic activity (*20*), but the question remained whether this concept applied to the enzymatic reaction. Binding of CO to FeMo cofactor was first visualized in 2014 by adding CO to the enzyme under turnover conditions (*21*). CO bound in a μ$_2$-bridging fashion at Fe2 and Fe6, reversibly replacing one of the characteristic belt sulfides of the cluster, S2B (Fig. 1C). From here, a debate ensued whether this structure revealed the long-sought N_2 binding site or represented an off-pathway inhibited state. The observed binding of selenide in FeMo cofactor (*22*) and a reaction intermediate in FeV cofactor (*23*) have since supported the relevance of ligand binding to Fe2 and Fe6, and the reversible replacement of S2B was recognized as essential to the mechanism (*11*). Most recently, a CO complex of FeV cofactor was also only obtained under turnover conditions (Fig. 1D) (*24*). The highly similar binding of CO to both clusters did not explain their difference in reactivity toward CO, in particular, because C-C bond formation implies the binding of two molecules of CO during the reaction (*25*). In line with this, electron paramagnetic resonance and infrared (IR) spectroscopy identified distinct CO binding events to FeMo cofactor, reported as a low-CO and a high-CO

[1]Institute for Biochemistry, University of Freiburg, Albertstrasse 21, 79104 Freiburg, Germany. [2]Institute of Chemistry, Technical University of Berlin, Straße des 17. Juni 135, 10623 Berlin, Germany. [3]Institute of Experimental Physics, Department of Physics, Free University of Berlin, Arnimallee 14, 14195 Berlin, Germany.
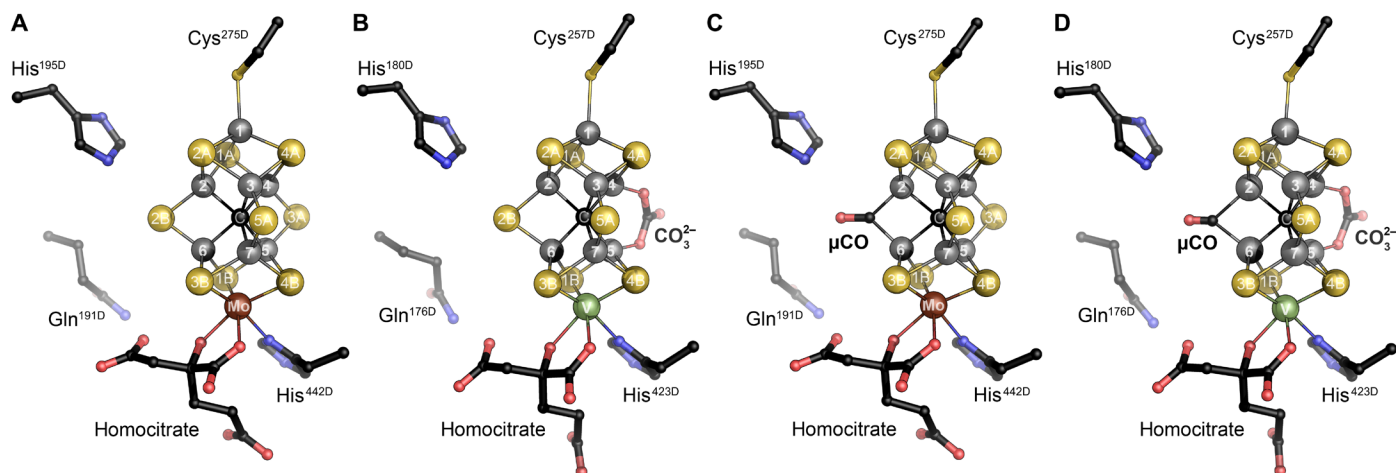*Corresponding author. Email: einsle@biochemie.uni-freiburg.de

Fig. 1. The active site cofactor of the two structurally characterized nitrogenases. (**A**) FeMo cofactor in the resting state E_0 [extended data, Fig. 5; Protein Data Bank (PDB) 3U7Q] (*62*). (**B**) FeV cofactor in the resting state (PDB 5N6Y) (*6*). (**C**) FeMo cofactor in the CO-inhibited state (PDB 4TVK) (*21*). (**D**) FeV cofactor in the low-CO state (PDB 7ADR) (*24*). All atoms of the cofactors are labeled according to standard convention.

state (*26–33*). As a peculiarity of V nitrogenase, these CO states were reportedly formed by pressurization in the presence of the reductant Eu(II)– diethylenetriamine pentaacetic acid, but without requiring Fe protein and ATP (*34*). However, we only obtained a stable low-CO state under turnover conditions (*24*), and a second ligand could not be visualized following this protocol. Thus, we have pressurized crystals of V nitrogenase in the low-CO state with 1.5 atm CO for 1 min, followed by rapid freezing for diffraction data collection.

RESULTS

V nitrogenase VFe protein from *Azotobacter vinelandii* crystallized in the monoclinic space group *P*1 with one $VnfD_2K_2G_2$ heterohexamer per unit cell (*6*) and turnover of the enzyme in presence of CO had yielded high-quality crystals of the low-CO state (Fig. 1D) (*24*). The further pressurization of these crystals was mostly detrimental for their diffraction properties, but we eventually recorded a dataset of the high-CO state to 1.05 Å resolution (table S1). The refined structure aligned with the one for the low-CO state with a root mean square deviation of only 0.064 Å and showed no substantial differences other than at the two copies of FeV cofactor in the unit cell. In the electron density maps, the μ_2-bridging CO ligand at Fe2 and Fe6, subsequently denoted as μCO, was fully occupied with no indication for remaining sulfide S2B (Fig. 2A) (*21*). In addition, a previously unobserved, elongated electron density maximum was apparent at iron Fe6 in both FeV cofactors of the protein that had not been present in the low-CO state. The magnitude of the electron density feature indicated that the binding site was only partially occupied, and at an occupancy of $q = 0.5$, it accommodated a second, terminal CO molecule, hereafter tCO, very well and with an Fe-C bond distance of 1.89 Å (Fig. 2B). The binding geometry was almost perfectly linear, with an Fe6-C-O angle of 179.3°, and nearly collinear with the central carbide [$C_{(carbide)}$-Fe6-$C_{(CO)}$ angle of 167.0°]. The binding mode of the two CO ligands in this high-CO state thus differs from the two terminal carbonyls predicted originally (*28*) but is similar to one of the models derived from IR spectroscopic studies (*35*). While μCO remained a ligand to Fe2 and Fe6, the additional tCO was exclusively observed at Fe6, at variance with reports of multiple CO ligands in
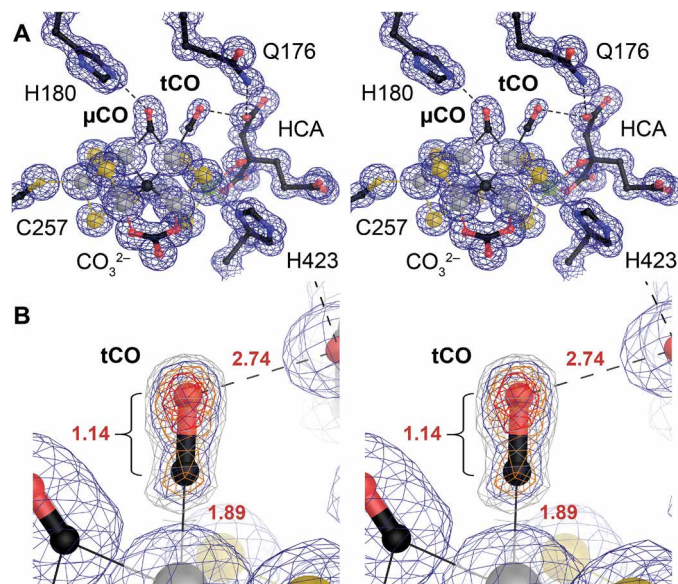

Fig. 2. The high-CO state of V nitrogenase. (**A**) Stereo image showing a $2F_o–F_c$ difference electron density map in the vicinity of FeV cofactor, contoured at the 2σ level. The μ_2-bridging μCO ligand is modeled at full occupancy q, the terminal tCO ligand at Fe6 is modeled with $q = 0.5$. (**B**) Detail of the bound tCO molecule at Fe6 (stereo image). The electron density map is contoured at 1σ (gray), 2σ (blue), 3σ (orange), and 3.5σ (red) to highlight the distinct maxima for the C and O atoms and their different electron density peak heights. Distances are given in Ångstrøm (10^{-10} m).

the high-CO state (*34*). This is easily rationalized for Fe4 and Fe5 that are bridged by a sterically more demanding carbonate ligand (fig. S2). Among the remaining sites, Fe2 is also directly adjacent to μCO, but here, access is blocked by the imidazole moiety of residue H180, an essential histidine thought to serve as proton donor during substrate reduction (*11*). The same is not true for the remaining Fe positions, Fe3 and Fe7, that are bridged by sulfide S5A. Although there are amino acid side chains in the vicinity (the aryl ring of F211[D] at 4.14 Å to Fe3 and the N_ζ nitrogen of K83[D] at 3.78 Å to Fe7), there

is no obvious steric hindrance, with one coordinated water molecule located above each iron site (fig. S2). For FeMo cofactor, spatially refined anomalous dispersion analysis of the resting state showed that Fe3 and Fe7 are the most reduced sites and should therefore be less favored by the nucleophilic CO ligand (*17*). It is, so far, unclear whether FeV cofactor has the same electronic structure and how the CO-bound states compared with the resting state. However, an important difference is the vicinity of the bridging μCO at Fe6, while Fe3 and Fe7 remain bridged by the soft sulfide ligand that may reduce the electrophilicity of an adjacent Fe. The selective binding of tCO thus further supports the uniqueness of the Fe2-Fe6 edge as a substrate binding site.

The true atomic resolution of the low-CO [d_{min} = 1.0 Å, (*24*)] and high-CO (d_{min} = 1.05 Å) states allowed for a structure refinement with minimal weight on geometric restraints so that the observed configurations can be compared in high detail. As expected, the binding of tCO as a terminal ligand to Fe6 increases the bond length in trans, from the central carbide to Fe6, from 2.00 Å in the low-CO state to 2.02 Å in the high-CO state (Fig. 3, A to C). This is accompanied by a shift of the carbide itself by 0.07 Å toward Fe6, while Fe2, Fe3, Fe4, Fe5, and Fe7 retain their exact positions. Furthermore, the binding of tCO has a measurable effect on the position of the μCO that shifts away from Fe6, thereby extending its bond length from 1.96 Å in the low-CO state to 2.02 Å in the high-CO state, in conjunction with a shortening of the Fe2-C$_{(\mu CO)}$ bond from 2.05 to 1.99 Å (Fig. 3). The C$_{(tCO)}$-Fe6-C$_{(\mu CO)}$ angle is 66.2°, bringing the carbon atoms of both CO ligands into close proximity (2.14 Å). In effect, the binding of tCO thus pulls Fe6 slightly out of the cluster and shifts μCO toward Fe2 and H180, where the H-bond from its N$_{\varepsilon 2}$ to O$_{(CO)}$ contracts from 2.87 Å in the low-CO state to 2.74 Å in

the high-CO state. Note, however, that tCO is modeled with an occupancy of q = 0.5, implying that the structure still represents a mixture of the low-CO and the high-CO states. Although the electron density maxima for the central carbide and Fe6 appear perfectly spherical, the structure may reflect this fact in the refined anisotropic temperature factors U_{ij}, where only in the high-CO state a displacement of the μCO oxygen is visible that corresponds to its positional shift from the low-CO state (fig. S3). As a result, μCO does not show distinct maxima for the C and O atoms, while tCO does, even at its reduced occupancy. The tCO triple bond refined to 1.14 Å, in line with terminal carbonyls that are elongated with respect to free CO at 1.128 Å. This finding was corroborated by in situ attenuated total reflectance (ATR) IR difference spectroscopy, where an additional absorption with a stretching frequency of v_{CO} = 1931 cm^{-1} appeared in the presence of 1 atm ^{12}CO upon incubating a previously adjusted low-CO state (Fig. 3D and fig. S4, A and B). The signal built up to saturation over 60 s but disappeared swiftly when the CO atmosphere was replaced by N$_2$ (Fig. 3, E and F). Steady-state accumulation of the high-CO state was achieved at 0.5 bar ^{12}CO overpressure. When the sample was afterward pressurized with ^{13}CO, the band shifted to 1888 cm^{-1}, unambiguously confirming the CO assignment (Fig. 3D). The μCO band was less clearly visible, as bridging carbonyls show lower stretching frequencies often overlaid by the strong absorptions of liquid water and the protein backbone (amide I) (*36*). However, the ^{12}CO/^{13}CO exchange experiment allowed generating difference spectra that revealed tentative signals for μ^{12}CO and, potentially, μ^{13}CO (fig. S4C).

Our data confirmed that the high-CO state was stabilized under CO pressure and that the characteristic tCO ligand was lost upon pressure release (Fig. 3F). Conversely, the μ_2-bridging μCO ligand
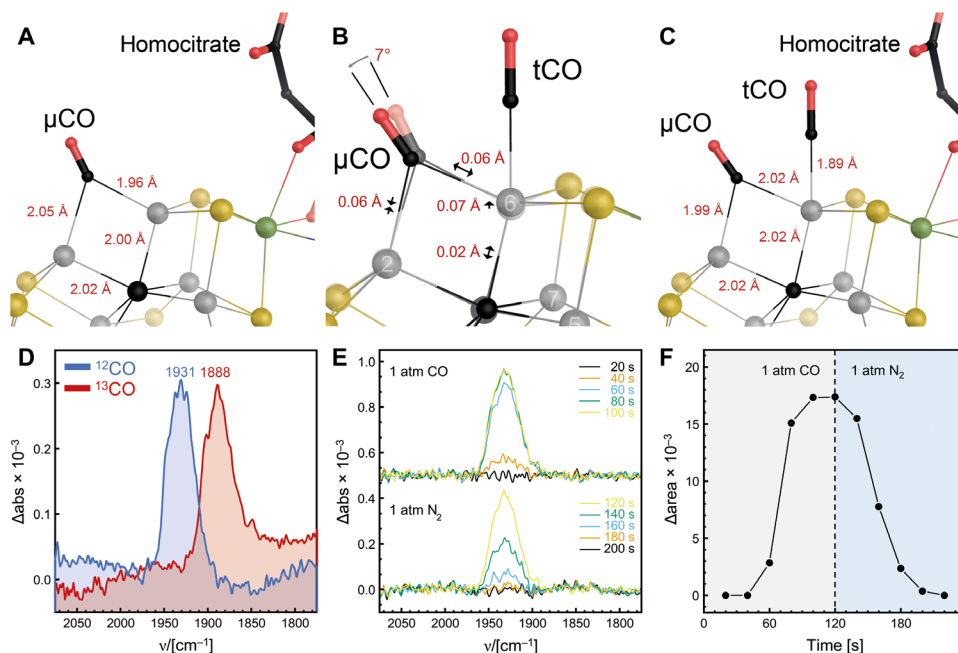

Fig. 3. Binding of the second CO ligand. (**A**) Bond distances around the μ_2-bridging CO ligand in the low-CO state of V nitrogenase. (**B**) Changes in bond distances and angles upon binding of the second CO ligand, as a terminal carbonyl to Fe6. Note that due to the 7° rotation of μCO, the hydrogen bond from its oxygen atom to residue H180 contracts from 2.87 to 2.74 Å. (**C**) Bond distances in the high-CO state of V nitrogenase. (**D**) IR difference spectra for ^{12}CO and ^{13}CO versus N$_2$-pressurized VFe protein. The distinct signals are in a typical range for terminal carbonyls and show an isotope shift of 43 cm^{-1}. (**E**) Kinetics of ^{12}tCO binding (above) and dissociation (below). (**F**) The time course for (D) shows not only rapid binding but also rapid dissociation of CO from the tCO site.

was stable for weeks, and its removal required turnover in the presence of Fe protein and ATP (*24*). In addition, the binding modes of μCO observed for Mo and V nitrogenase are virtually identical, despite a difference of nearly three orders of magnitude in CO-reducing activity. While stopped-flow IR spectroscopy with the MoFe protein of *Klebsiella pneumoniae* had indicated an accumulation of μCO already at 0.02 bar CO (*37*), we observed μCO binding to *A. vinelandii* VFe protein at 1 and 5 bar pCO, but not at 0.02 bar. If the observed binding mode of μCO was a thermodynamically trapped adduct, then it should also accumulate at low CO pressure. As a substrate, however, it can be reduced, reopening the binding site at Fe2-Fe6 and diverting further electron flux toward unproductive H_2 formation (hydride protonation). This differentiation is of high mechanistic relevance. Following the catalytic scheme of Thorneley and Lowe (*38*), nitrogenase binds CO only after two-electron reduction to the E_2 state (Fig. 4 and fig. S5), but μCO is still a carbonyl so that, at this point, it is the cofactor that should be two-electron–reduced. This is at variance with the current understanding that electron flux from Fe protein can only reduce the cofactor by one electron, while the second reducing equivalent invariably leads to hydride formation at the cluster surface (*9, 39*), suggested to replace sulfide S2B at Fe2 and Fe6 [Fig. 4 (**2**)] (*11, 23, 40*). Thus, either the two electrons remain as a terminal hydride on the cluster [Fig. 4 (**3**)] or the bridging binding of CO only occurs after protonation of the hydride and its loss as H_2 [Fig. 4 (**4**)]. In the first case, a less stable terminal hydride is highly unlikely to persist for the time of our analysis (*41, 42*). In the second case, however, CO replaces the bridging hydride of the E_2 state and the loss of H_2 returns the cluster to its resting state E_0 [Fig. 4 (**4**)].

From here, two reduction steps can lead back to E_2, either releasing the CO ligand and reactivating the enzyme [Fig. 4 (**3 → 2**)] or leading once more to hydride protonation and H_2 release [Fig. 4 (**3 → 4**)], which explains why CO binding inhibits all catalysis other than H_2 formation. Accordingly, we conclude that μCO is not an intermediate of CO reduction but a reversibly inhibited state for both Mo and V nitrogenase (*21, 24*). Similarly, the binding of tCO as observed here also does not represent an intermediate of CO reduction. It is not a redox-dependent event at all: Binding is reversible as shown by IR spectroscopy (Fig. 3, E and F) and was only achieved by in situ pressurization [Fig. 4 (**6**)].

We hypothesize that for productive reduction of CO, the enzyme must use the reducing power of the bound hydride in E_2 rather than losing it to protonation. In full analogy to Fischer-Tropsch chemistry, this can be achieved by an insertion of CO into the bound hydride, leading to a formyl adduct [Fig. 4 (**5**)]. With the definition of two binding sites, a μ-site bridging Fe2 and Fe6 and the t-site at Fe6 found in this study, a repeated cycle of reduction, hydride formation at the t-site and hydrogenation of the ligand at the μ-site, emerges as a common principle of nitrogenase functionality. It provides a framework for CO reduction in consecutive two-electron steps and explains why ethylene rather than methane is the main product (fig. S6). The eight-electron reduction of two CO molecules to yield ethylene is initiated if a bound CO ligand undergoes an insertion reaction [Fig. 4 (**3 → 5**) and fig. S6 (**1 → 2**)] to yield a formyl adduct at Fe2 with the cluster formally in the E_0 state. The continuing electron influx from Fe protein brings the system back to E_2, when another hydride is formed in the t-site [fig. S6 (**3**)]. The following hydrogenation
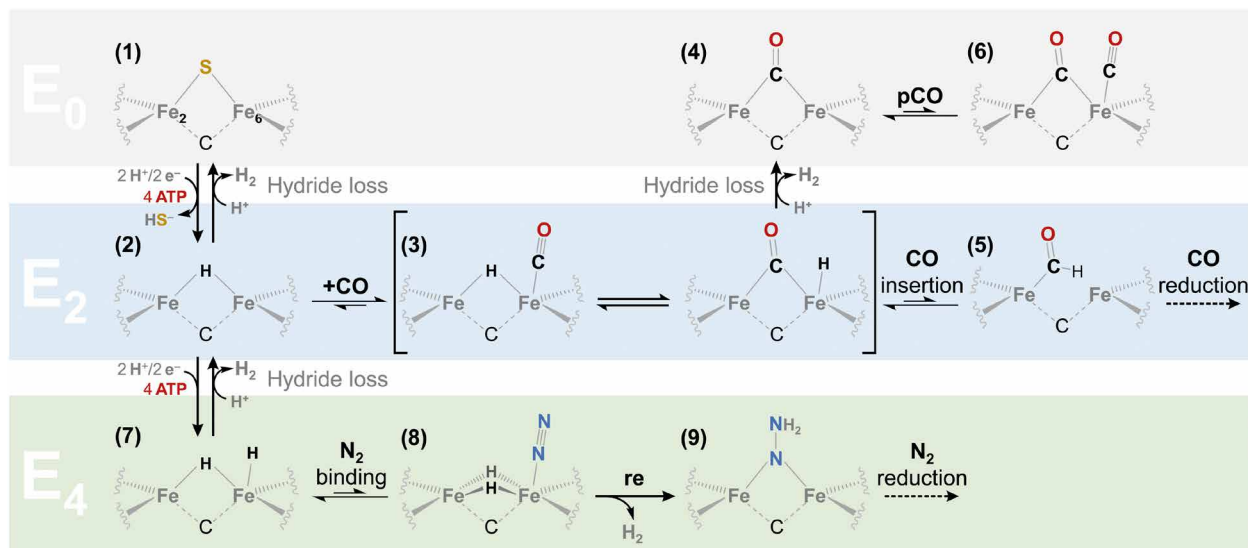

Fig. 4. Mechanistic implications for the different reactivities of nitrogenases. Nitrogenase catalysis according to the kinetic scheme of Thorneley and Lowe (extended data, Fig. 5) proceeds along successive e^-/H^+ transfer steps from the resting state E_0 (**1**) to a hydride-bridged state E_2 (**2**). Here, CO can bind to the cofactor, and we propose an initial terminal binding to Fe6 that is in equilibrium with a bridging carbonyl and a terminal hydride (**3**). The protonation of the unstable terminal hydride leads to release of H_2, with the $μ_2$-bridging carbonyl remaining in a formal E_0 state that was characterized structurally and spectroscopically as "low-CO" state (**4**). Alternatively, productive CO reduction by VFe protein may be initiated by an insertion reaction to yield a formyl adduct as a first step (**5**), while in this work, we show that pressurization of (**4**) leads to the "high-CO" state (**6**) that reveals Fe6 as the site for the terminal binding of ligands. While the two CO-bound states (**4**) and (**6**) likely are not on path for CO reduction, the concurrent bridging and terminal binding of two ligands rationalizes the mechanistically critical step (**3**) and also provides a new outlook on the initial steps of N_2 activation. These require the enzyme to reach the E_4 state that holds two hydrides. If one of these is bridging and the other terminal (**7**) in analogy to the high-CO state (**6**), then terminal N_2 binding to Fe6 could force a shift of the terminal hydride to become bridging, triggering the reductive elimination (re) of H_2 only after the substrate is in position (**8**) and leaving the enzyme in a super-reduced state that transfers two electrons to N_2, effectively breaking the stable triple bond of dinitrogen (**9**). The schemes depict a fragment of the cofactor including Fe sites Fe2 and Fe6 and the interstitial carbide (C).

leads to bound methanol, for which the conserved H180 provides a proton [fig. S6 (**4**)]. In the second cycle of reduction and hydrogenation [fig. S6 (**5**)], the bound ligand is reduced to the methyl stage and water is released [fig. S6 (**6**)]. The dissociation of methane at this stage is not favored, and instead, the reaction progresses toward C-C coupling with the binding of a second CO molecule that does not require a reduced state once the μ-sulfide S2B is displaced [fig. S6 (**7**)]. The tCO then inserts into the bound methyl group in a reaction reminiscent of the nickel-containing acetyl–coenzyme A synthase that also results in a metal-bound acetyl group [fig. S6 (**8**)] (*43*). Note that a subpopulation of this enzyme also binds a second CO to its nickel site (*44*). With two further reduction steps to a terminal hydride at Fe6 [fig. S6 (**9**)], a third hydrogenation leads to bound ethanol [fig. S6 (**10**)], and in a final cycle of reduction and hydride formation [fig. S6 (**11**)], this results in a bound ethyl group and water release [fig. S6 (**2**)]. From this point, the ethyl group [other than the methyl in (**6**)] can undergo β-elimination of a hydride, as postulated for product release in Fischer-Tropsch reactions (*45*). It releases the product ethylene and retains an enzyme-bound hydride, i.e., the E_2 state of the system (fig. S6C). Alternatively, the binding of another tCO may outcompete the elimination reaction and lead to another cycle of chain elongation that then leads to propylene, C_3H_6, or propane, C_3H_8, as a C_3 product (*16*). The main product of CO reduction by Fe nitrogenase was reported to be methane (*25*), implying that this enzyme has the possibility to release product at stage (**6**). A rationalization of this finding will likely have to await the structural characterization of this final class of nitrogenases.

DISCUSSION

The terminal CO ligand coordinates weakly, and its binding to FeV cofactor is only observed after sulfide S2B, a distinct weak-field ligand, is replaced by a strong-field ligand at the μ-site. Our data show that the t-site at Fe6 marks a defined second position on the cofactor for the terminal binding of a small ligand. This concept can be generalized beyond the reduction of CO, as the hydride anion is an equally strong σ-donor ligand. H^- and CO adopt similar binding modes and ligand replacement from μ-CO to μ-H is well established from model complexes (*46*) and hydrogenase enzymes (*47–52*), making CO a bona fide indicator for hydride binding sites. The similarity of μCO and a $μ_2$-hydride suggests that the establishment of the first $μ_2$-H in E_2 is a strict prerequisite for ligand binding at the t-site, but it also indicated that the very first binding event always occurs at the t-site. During nitrogenase catalysis, electrons accumulated at Fe2 and/or Fe6, favoring the formation of a terminal hydride that likely subsequently rearranges to a more stable μH [Fig. 4 (**2**)]. We have previously suggested the conserved H180 as a proton conduit during the reaction, but the mechanism outlined above (fig. S6) implies that this residue only provides the protons that are transferred to the distal atom of a diatomic substrate, while the proximal atom receives the hydrides from Fe6. As reaction intermediates coordinate to H180, the enzyme will require a second proton source in close vicinity to Fe6. Multiple proton transfer pathways in nitrogenase have been investigated by theoretical methods, with a preference for a Grotthuss-type proton relay terminating at the homocitrate ligand or sulfur S3B that coordinates Fe6 (*53*). If so, all hydride formation may consistently start with a terminal hydride at Fe6, by abstracting a proton from the α-carboxylate or, more likely, the 3′-OH group of homocitrate that is protonated in the resting state (*54*) upon transfer

of the second electron from Fe protein. The physiological reduction of N_2 requires the E_4 state to be reached, and the terminal hydride will migrate to the μ-site, where it is sufficiently stabilized to persist, vacating the t-site for the formation of the second hydride. For CO reduction, however, this is not possible: In the low-CO state the μ-site is occupied with CO [Fig. 4 (**4**)], and terminal hydrides will eventually be lost to protonolysis, yielding unwanted H_2. If, on the other hand, CO successfully inserts into a μH, CO reduction can proceed (fig. S6), with the enzyme reiterating its task of hydride formation at the t-site that then leads to continued reduction of the bound carbon species, preventing the enzyme from ever reaching the desired E_4 state required for N_2 reduction.

Although CO reduction is centered on the enzyme cycling between the E_0 and E_2 states (fig. S5), the description of a μ- and a t-site at the cofactor is valuable for understanding N_2 reduction. When the enzyme reaches the E_4 state, it will do so with a bridging μH, stabilized by interaction with the inward-facing Q176 and a terminal tH at Fe6 [Figs. 4 (**7**), and 5A]. Although a terminal hydride is less stable and protonolysis via homocitrate may occur (Fig. 5B), retaining it at the t-site prevents the reductive elimination of H_2 in the absence of substrate. Upon N_2 binding, however, the doubly bridging arrangement of two hydrides readily promotes reductive elimination [Figs. 4 (**7**) and 5C]. How realistic is this proposed intermediate (**7**)?

Rittle *et al.* reported a diiron model compound with two stable hydrides bridging the metals (Fig. 5D). A terminal N_2 ligand stably bound to one Fe site at room temperature, and the binding affinity was increased 10^6-fold upon reduction from a $Fe^{II}(μ_2$-H)Fe^{II} form to a mixed-valent state. Adding proton and electron sources, the authors observed the formation of NH_3 (*55*). The high-CO state of V nitrogenase may be a biological analog to this complex, albeit with CO as a stand-in for hydride. In E_2, the enzyme is not sufficiently activated to bind N_2, but the far stronger ligand tCO can model the N_2 binding event that only occurs once E_3 or E_4 are reached. We have suggested that in E_2, sulfide S2B is already relocated to its holding site, triggering residue Q176 to attain an inward-facing conformation that stabilizes a single $μ_2$-H (*11*). In the high-CO state structure, the two CO ligands do not accommodate Q176 in the inward-facing state, resulting in the observed loss of S2B. However, this would not apply for two hydrides: If the E_4 state featured a bridging hydride at Fe2 and Fe6 as well as a terminal hydride at Fe6 [Figs. 4 (**7**) and 5A], residue Q176 could still face inward. This would stabilize the E_4 state, preventing proton transfer via H180 and the reductive elimination of H_2. Binding of N_2 to Fe6 as an initial point of contact, in analogy to tCO, would then interfere with Q176 and force the migration of the terminal hydride into a bridging position, highly similar to the Rittle/Peters complex [Figs. 4 (**8**) and 5C]. With the protective interaction with Q176 removed and due to the rigidity of the cofactor, the two hydrides will recombine and eliminate H_2, generating the super-reduced E_4^* state that is able to break the triple bond of N_2 [Fig. 4 (**9**)] (*23*).

In conclusion, the discovery of a second specific ligand binding site on FeV cofactor has wide-ranging mechanistic implications. It helps to rationalize an initial end-on binding event not only for substrates such as N_2 and CO but also for the protons that form the surface hydrides at the heart of the nitrogenase mechanism. Originating as a terminal ligand, these hydrides will displace sulfide S2B and migrate to the more stable μ-site, as an essential prerequisite to extend their lifetime until the next reduction occurs from Fe protein. Once the weak-field ligand sulfide is removed, both CO and μH at
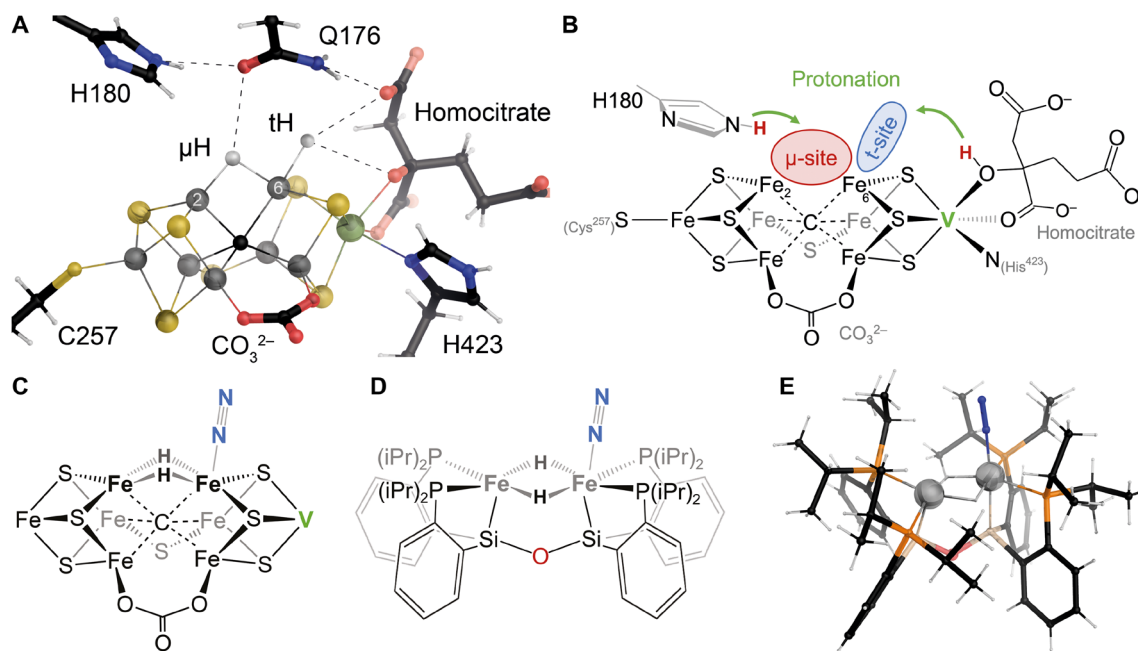
Fig. 5. Implications for N₂ reduction by nitrogenase. (**A**) Hypothetical E_4 state with hydrides at the μ- and the t-site. Although highly energetic, the state is stabilized by Q176 interacting with the μH. (**B**) Schematic view of FeV co with the μ- and t-sites highlighted. While H180 serves as proton donor for intermediates bound to the μ-site or Fe2, the t-site is likely supplied with H^+ from the hydroxyl group of homocitrate. (**C**) The mechanistic suggestion of a doubly dihydride-bridged cofactor in the E_4 state [Fig. 4, (**8**)] is not without precedent. (**D**) The N₂-bound diiron complex $(Fe_2(\mu-H)_2-N_2)[SiP_2O]$ reported by Rittle and Peters (*55*) affords a highly similar topology. The compound was stable at room temperature and reversibly bound a second terminal N₂ at the other Fe site upon cooling to 193 K. Reduction to a mixed-valent $Fe^{II}:Fe^{I}$ state led to a 10^6-fold rate enhancement of N₂ binding. (**E**) The crystal structure of (D) reveals that the μ_2-hydrides are juxtaposed, likely adding to their stability. In contrast, nitrogenase cofactors are more rigid due to the remaining belt ligands, possibly imposing a Fe-Fe distance and geometry that favors the reductive elimination of H_2, as soon as the binding of N₂ displaces the tH to a bridging position.

the μ-site promote further ligand binding at the t-site. This concept unifies the seeming distinct reductions of one N₂ to two NH_4^+ and of two CO into a common mechanism of hydride formation and stabilization that gives the enzyme nitrogenase its unmatched capacity to reduce even the most stable of substrates at ambient conditions.

MATERIALS AND METHODS
Protein production and isolation
V nitrogenase was purified anoxically from *A. vinelandii* according to a previously described procedure (*56*). Briefly, cultures of *A. vinelandii* were grown under molybdenum depletion, and vanadium was used as supplement. All purification steps were carried out either in a sealed chamber containing a N_2/H_2 gas mixture (95:5) or by use of modified Schlenk techniques under N₂ gas. The purification procedure comprised two consecutive anion exchange chromatography steps and a final size exclusion chromatography step. The two components of the enzyme were separately obtained in buffer containing 100 mM NaCl, 2.5 mM sodium dithionite, and 50 mM tris-HCl buffer at pH 7.4. Proteins were flash-frozen and stored in liquid nitrogen until further use.

CO turnover
Low electron flux CO turnover was carried out according to published procedures (*24*). Assay solutions contained 5 mg ml⁻¹ VnfDKG, 0.5 mg ml⁻¹ VnfH, 20 mM tris-HCl (pH 7.4), 10 mM MgCl₂, 15 mM phosphocreatine, 0.125 mg ml⁻¹ phosphocreatine kinase, and 25 mM sodium dithionite. Samples were purged with carbon monoxide and

incubated for 3 min at 30°C and 320 rpm under agitation. ATP was added as the last step to reach a final concentration of 2.5 mM ATP. Samples were continuously agitated at 30°C and 320 rpm for at least 1 hour. Carbon monoxide was subsequently removed from the sample for crystallization under an N_2/H_2 atmosphere (95:5).

Crystallization and CO pressurization
VnfDKG was crystallized according to the previously published protocols (*6, 24*) by sitting drop vapor diffusion in 24-well crystallization plates (Cryschem). ZnCl₂ was added to the protein solution to reach a concentration of 0.1 mM ZnCl₂, and 2 μl of this protein solution was mixed with 2 μl of reservoir solution for each drop. Reservoir solutions contained 100 mM tris-HCl (pH 7.5), 30 mM MgCl₂, 20% (v/v) ethylene glycol, 7 to 12% (w/v) polyethylene glycol 8000, and 1 mM sodium dithionite. Amount and shape of crystals were subsequently optimized by addition of 0.5 μl of microseeds to each drop. Crystals were grown for 1 to 2 weeks. Single crystals were harvested with a nylon loop and incubated shortly in 2-μl drops of fresh reservoir solution containing 2 mM sodium dithionite. Crystals were then mounted into a pressure chamber (Xcell, Oxford Cryosystems), and a pressure of 2.5 bar CO was applied at room temperature. After 60 s, pressure was slowly released. The chamber was quickly opened, and crystals were flash-frozen in liquid nitrogen.

Data collection and refinement
Data collection was carried out at the Swiss Light Source (Paul Scherrer Institute, Villigen, Switzerland) at beamline X06DA (PXIII) equipped with a Pilatus 2 M-F detector (Dectris). XDS (*57*) was used for

indexing and integration and Aimless from the CCP4 suite (58) for merging and scaling. The previously obtained CO-bound structure was modified using Coot (59). REFMAC5 (60) was used for structure refinement with anisotropic temperature factors and ligand dictionary files from previous published structures (23). For the refined structure, the maximum likelihood–based estimated standard uncertainty for atom positions was 0.019 Å, and only changes exceeding this value are discussed in the manuscript. Figures were generated with PyMOL (Schrödinger).

IR spectroscopy

IR spectroscopic measurements were performed under dry and strictly anoxic conditions, in the dark, and at room temperature. The Fourier transform spectrometer (Tensor27, Bruker) was equipped with an ATR element including an Si microcrystal with two active reflections (Dura SamplIR II, Smith Detection). A custom-made polychloro-trifluoroethylene (PCTFE) lid with a manometer and various gas inlets was screwed onto the DuraDisc and connected to N_2, ^{12}CO, and ^{13}CO gas sources. This setup allowed for time-resolved in situ gas exchange experiments, as reported previously (61). All absorbance spectra were recorded with a spectral resolution of 2 cm^{-1}, which facilitated a temporal resolution of 10 to 20 s for an average of 50 to 100 interferometer scans (80 kHz). For this, a low-noise background (1000 scans) was taken on the "empty" ATR crystal. Then, 1 μl of nitrogenase solution (~0.5 mM) was pipetted onto the Si mircocrystal and carefully dried under N_2 for typically 120 to 180 s. Afterward, the gas was sent through a wash bottle containing 50 mM tris-HCl (pH 8) and ~5 mM sodium dithionite to create an aerosol that was used to rehydrate the nitrogenase film, as described previously (61). N_2/CO exchange experiments were performed at ambient pressure (~1 atm) and a continuous exchange of the gas atmosphere, whereas the ^{12}CO/^{13}CO isotope editing was conducted under an overpressure of 0.5 bar (equivalent to ~1.5 atm). Difference spectra were calculated in OPUS software (Bruker) and fitted using a home-written routine, as described previously (61).

Note added in proof: We have become aware of a similar study concerning the binding of CO to a different class of nitrogenases, the Mo nitrogenase. The study, "Structural characterization of two CO molecules bound to the nitrogenase active site" was published by T. M. Buscagan, K. A. Perez, A. O. Maggiolo, D. C. Rees, T. Spatzal; Angew Chem Int Edit 60, 5704–5707 (2021).

SUPPLEMENTARY MATERIALS
Supplementary material for this article is available at http://advances.sciencemag.org/cgi/content/full/7/22/eabg4474/DC1

REFERENCES AND NOTES
1. P. W. Wilson, R. H. Burris, The mechanism of biological nitrogen fixation. *Bacteriol. Rev.* **11**, 41–73 (1947).
2. B. K. Burgess, D. J. Lowe, Mechanism of molybdenum nitrogenase. *Chem. Rev.* **96**, 2983–3012 (1996).
3. O. Einsle, D. C. Rees, Structural enzymology of nitrogenase enzymes. *Chem. Rev.* **120**, 4969–5004 (2020).
4. Y. Hu, M. W. Ribbe, Historic overview of nitrogenase research. *Methods Mol. Biol.* **766**, 3–7 (2011).
5. O. Einsle, Nitrogenase FeMo cofactor: An atomic structure in three simple steps. *J. Biol. Inorg. Chem.* **19**, 737–745 (2014).
6. D. Sippel, O. Einsle, The structure of vanadium nitrogenase reveals an unusual bridging ligand. *Nat. Chem. Biol.* **13**, 956–960 (2017).
7. R. R. Eady, Structure-function relationships of alternative nitrogenases. *Chem. Rev.* **96**, 3013–3030 (1996).
8. D. F. Harris, D. A. Lukoyanov, S. Shaw, P. Compton, M. Tokmina-Lukaszewska, B. Bothner, N. Kelleher, D. R. Dean, B. M. Hoffman, L. C. Seefeldt, Mechanism of N_2 reduction catalyzed by Fe-Nitrogenase involves reductive elimination of H_2. *Biochemistry* **57**, 701–710 (2018).
9. L. C. Seefeldt, Z.-Y. Yang, D. A. Lukoyanov, D. F. Harris, D. R. Dean, S. Raugei, B. M. Hoffman, Reduction of substrates by nitrogenases. *Chem. Rev.* **120**, 5082–5106 (2020).
10. B. M. Hoffman, D. Lukoyanov, D. R. Dean, L. C. Seefeldt, Nitrogenase: A draft mechanism. *Acc. Chem. Res.* **46**, 587–595 (2013).
11. M. Rohde, D. Sippel, C. Trncik, S. L. A. Andrade, O. Einsle, The critical E_4 state of nitrogenase catalysis. *Biochemistry* **57**, 5497–5504 (2018).
12. D. F. Harris, D. A. Lukoyanov, H. Kallas, C. Trncik, Z.-Y. Yang, P. Compton, N. Kelleher, O. Einsle, D. R. Dean, B. M. Hoffman, L. C. Seefeldt, Mo-, V-, and Fe-nitrogenases use a universal eight-electron reductive-elimination mechanism to achieve N_2 reduction. *Biochemistry* **58**, 3293–3301 (2019).
13. J. C. Hwang, C. H. Chen, R. H. Burris, Inhibition of nitrogenase-catalyzed reductions. *Biochim. Biophys. Acta* **292**, 256–270 (1973).
14. C. C. Lee, Y. L. Hu, M. W. Ribbe, Vanadium nitrogenase reduces CO. *Science* **329**, 642–642 (2010).
15. Q. H. Zhang, K. Cheng, J. C. Kang, W. P. Deng, Y. Wang, Fischer-Tropsch catalysts for the production of hydrocarbon fuels with high selectivity. *ChemSusChem* **7**, 1251–1264 (2014).
16. C. C. Lee, K. Tanifuji, M. Newcomb, J. Liedtke, Y. Hu, M. W. Ribbe, A comparative analysis of the CO-reducing activities of mofe proteins containing Mo- and V-nitrogenase cofactors. *Chembiochem* **19**, 649–653 (2018).
17. T. Spatzal, J. Schlesier, E. M. Burger, D. Sippel, L. Zhang, S. L. A. Andrade, D. C. Rees, O. Einsle, Nitrogenase FeMoco investigated by spatially resolved anomalous dispersion refinement. *Nat. Commun.* **7**, 10902 (2016).
18. N. P. Mankad, M. T. Whited, J. C. Peters, Terminal Fe^I–N_2 and Fe^{II}···H–C interactions supported by tris(phosphino)silyl ligands. *Angew. Chem. Int. Ed.* **46**, 5768–5771 (2007).
19. J. Rittle, J. C. Peters, Fe-N_2/CO complexes that model a possible role for the interstitial C atom of FeMo-cofactor (FeMoco). *Proc. Natl. Acad. Sci. U.S.A.* **110**, 15898–15903 (2013).
20. S. E. Creutz, J. C. Peters, Catalytic reduction of N_2 to NH_3 by an Fe-N_2 complex featuring a C-atom anchor. *J. Am. Chem. Soc.* **136**, 1105–1115 (2014).
21. T. Spatzal, K. A. Perez, O. Einsle, J. B. Howard, D. C. Rees, Ligand binding to the FeMo-cofactor: Structures of CO-bound and reactivated nitrogenase. *Science* **345**, 1620–1623 (2014).
22. T. Spatzal, K. A. Perez, J. B. Howard, D. C. Rees, Catalysis-dependent selenium incorporation and migration in the nitrogenase active site iron-molybdenum cofactor. *eLife* **4**, e11620 (2015).
23. D. Sippel, M. Rohde, J. Netzer, C. Trncik, J. Gies, K. Grunau, I. Djurdjevic, L. Decamps, S. L. A. Andrade, O. Einsle, A bound reaction intermediate sheds light on the mechanism of nitrogenase. *Science* **359**, 1484–1489 (2018).
24. M. Rohde, K. Grunau, O. Einsle, CO binding to the FeV cofactor of CO-reducing vanadium nitrogenase at atomic resolution. *Angew. Chem. Int. Ed.* **59**, 23626–23630 (2020).
25. D. F. Harris, E. Jimenez-Vicente, Z.-Y. Yang, B. M. Hoffman, D. R. Dean, L. C. Seefeldt, CO as a substrate and inhibitor of H$^+$ reduction for the Mo-, V-, and Fe-nitrogenase isozymes. *J. Inorg. Biochem.* **213**, 111278 (2020).
26. D. J. Lowe, R. R. Eady, R. N. F. Thorneley, Electron-paramagnetic-resonance studies on nitrogenase of *Klebsiella-pneumoniae*. Evidence for acetylene-nitrogenase and ethylene-nitrogenase transient complexes. *Biochem. J.* **173**, 277–290 (1978).
27. L. C. Davis, M. T. Henzl, R. H. Burris, W. H. Orme-Johnson, Iron-sulfur clusters in the molybdenum-iron protein-component of nitrogenase. Electron-paramagnetic-resonance of the carbon-monoxide inhibited state. *Biochemistry* **18**, 4860–4869 (1979).
28. H.-I. Lee, L. M. Cameron, B. J. Hales, B. M. Hoffman, CO binding to the FeMo cofactor of CO-inhibited nitrogenase: ^{13}CO and ^1H Q-band ENDOR investigation. *J. Am. Chem. Soc.* **119**, 10121–10126 (1997).
29. R. C. Pollock, H.-I. Lee, L. M. Cameron, V. J. DeRose, B. J. Hales, W. H. Orme-Johnson, B. M. Hoffman, Investigation of CO bound to inhibited forms of nitrogenase MoFe Protein by ^{13}C ENDOR. *J. Am. Chem. Soc.* **117**, 8686–8687 (1995).
30. S. J. George, G. A. Ashby, C. W. Wharton, R. N. F. Thorneley, Time-resolved binding of carbon monoxide to nitrogenase monitored by stopped-flow infrared spectroscopy. *J. Am. Chem. Soc.* **119**, 6450–6451 (1997).
31. L. M. Cameron, B. J. Hales, Investigation of CO binding and release from Mo-nitrogenase during catalytic turnover. *Biochemistry* **37**, 9449–9456 (1998).
32. Z. Maskos, B. J. Hales, Photo-lability of CO bound to Mo-nitrogenase from *Azotobacter vinelandii*. *J. Inorg. Biochem.* **93**, 11–17 (2003).
33. L. Yan, V. Pelmenschikov, C. H. Dapper, A. D. Scott, W. E. Newton, S. P. Cramer, IR-monitored photolysis of CO-inhibited nitrogenase: A major EPR-silent species with coupled terminal CO ligands. *Chem. Eur. J.* **18**, 16349–16357 (2012).
34. C. C. Lee, J. Wilcoxen, C. J. Hiller, R. D. Britt, Y. L. Hu, Evaluation of the catalytic relevance of the CO-bound states of V-nitrogenase. *Angew. Chem. Int. Ed.* **57**, 3411–3414 (2018).

35. L. Yan, C. H. Dapper, S. J. George, H. Wang, D. Mitra, W. Dong, W. E. Newton, S. P. Cramer, Photolysis of Hi-CO nitrogenase—Observation of a plethora of distinct CO species using infrared spectroscopy. *Eur. J. Inorg. Chem.* **2011**, 2064–2074 (2011).

36. A. Barth, Infrared spectroscopy of proteins. *Biochim. Biophys. Acta* **1767**, 1073–1101 (2007).

37. R. N. F. Thorneley, in *Nitrogen Fixation: From Molecules to Crop Productivity*, F. O. Pedrosa, M. Hungria, G. Yates, W. E. Newton, Eds. (Springer, 2000), pp. 39–40.

38. H.-I. Lee, M. Sørlie, J. Christiansen, T.-C. Yang, J. Shao, D. R. Dean, B. J. Hales, B. M. Hoffman, Electron inventory, kinetic assignment (E$_n$), structure, end bonding of nitrogenase turnover intermediates with C$_2$H$_2$ and CO. *J. Am. Chem. Soc.* **127**, 15880–15890 (2005).

39. D. Lukoyanov, Z.-Y. Yang, B. M. Barney, D. R. Dean, L. C. Seefeldt, B. M. Hoffman, Unification of reaction pathway and kinetic scheme for N$_2$ reduction catalyzed by nitrogenase. *Proc. Natl. Acad. Sci. U.S.A.* **109**, 5583–5587 (2012).

40. J. B. Varley, Y. Wang, K. Chan, F. Studt, J. K. Norskov, Mechanistic insights into nitrogen fixation by nitrogenase enzymes. *Phys. Chem. Chem. Phys.* **17**, 29541–29547 (2015).

41. S. Raugei, L. C. Seefeldt, B. M. Hoffman, Critical computational analysis illuminates the reductive-elimination mechanism that activates nitrogenase for N$_2$ reduction. *Proc. Natl. Acad. Sci. U.S.A.* **115**, E10521–E10530 (2018).

42. D. Lukoyanov, N. Khadka, Z.-Y. Yang, D. R. Dean, L. C. Seefeldt, B. M. Hoffman, Reductive elimination of H$_2$ activates nitrogenase to reduce the N≡N triple bond: Characterization of the E$_4$(4H) Janus intermediate in Wild-Type Enzyme. *J. Am. Chem. Soc.* **138**, 10674–10683 (2016).

43. T. I. Doukov, T. M. Iverson, J. Seravalli, S. W. Ragsdale, C. L. Drennan, A Ni-Fe-Cu center in a bifunctional carbon monoxide dehydrogenase/acetyl-CoA synthase. *Science* **298**, 567–572 (2002).

44. C. D. James, S. Wiley, S. W. Ragsdale, B. M. Hoffman, ^{13}C electron nuclear double resonance spectroscopy shows acetyl-CoA synthase binds two substrate CO in multiple binding modes and reveals the importance of a CO-binding "Alcove". *J. Am. Chem. Soc.* **142**, 15362–15370 (2020).

45. G. Henrici-Olivé, S. Olivé, Fischer-Tropsch synthesis molecular-weight distribution of primary products and reaction-mechanism. *Angew. Chem. Intl. Ed.* **15**, 136–141 (1976).

46. D. J. R. Brook, V. Lynch, T. H. Koch, Disproportionation of diiron nonacarbonyl in THF solution: Formation and structure of Fe(THF)$_4$[HFe$_3$(CO)$_{11}$]$_2$. *Inorg. Chem* **34**, 5691–5693 (1995).

47. B. J. Lemon, J. W. Peters, Binding of exogenously added carbon monoxide at the active site of the iron-only hydrogenase (CpI) from *Clostridium pasteurianum*. *Biochemistry* **38**, 12969–12973 (1999).

48. H. Ogata, Y. Mizoguchi, N. Mizuno, K. Miki, S.-i. Adachi, N. Yasuoka, T. Yagi, O. Yamauchi, S. Hirota, Y. Higuchi, Structural studies of the carbon monoxide complex of [NiFe] hydrogenase from *Desulfovibrio vulgaris* Miyazaki F: Suggestion for the initial activation site for dihydrogen. *J. Am. Chem. Soc.* **124**, 11628–11635 (2002).

49. E. J. Lyon, S. Shima, R. Boecher, R. K. Thauer, F.-W. Grevels, E. Bill, W. Roseboom, S. P. J. Albracht, Carbon monoxide as an intrinsic ligand to iron in the active site of the iron-sulfur-cluster-free hydrogenase H$_2$-forming methylenetetrahydromethanopterin dehydrogenase as revealed by infrared spectroscopy. *J. Am. Chem. Soc.* **126**, 14239–14248 (2004).

50. M. Senger, S. Mebs, J. Duan, F. Wittkamp, U. P. Apfel, J. Heberle, M. Haumann, S. T. Stripp, Stepwise isotope editing of [FeFe]-hydrogenases exposes cofactor dynamics. *Proc. Natl. Acad. Sci. U.S.A.* **113**, 8454–8459 (2016).

51. M. Winkler, M. Senger, J. Duan, J. Esselborn, F. Wittkamp, E. Hofmann, U.-P. Apfel, S. T. Stripp, T. Happe, Accumulating the hydride state in the catalytic cycle of [FeFe]-hydrogenases. *Nat. Commun.* **8**, 16115 (2017).

52. H. Ogata, K. Nishikawa, W. Lubitz, Hydrogens detected by subatomic resolution protein crystallography in a [NiFe] hydrogenase. *Nature* **520**, 571–574 (2015).

53. I. Dance, The pathway for serial proton supply to the active site of nitrogenase: Enhanced density functional modeling of the Grotthuss mechanism. *Dalton Trans.* **44**, 18167–18186 (2015).

54. L. Cao, O. Caldararu, U. Ryde, Protonation states of homocitrate and nearby residues in nitrogenase studied by computational methods and quantum refinement. *J. Phys. Chem. B* **121**, 8242–8262 (2017).

55. J. Rittle, C. C. L. McCrory, J. C. Peters, A 10^6-fold enhancement in N$_2$-binding affinity of an Fe$_2$(μ-H)$_2$ core upon reduction to a mixed-valence Fe^{II}Fe^I State. *J. Am. Chem. Soc.* **136**, 13853–13862 (2014).

56. D. Sippel, J. Schlesier, M. Rohde, C. Trncik, L. Decamps, I. Djurdjevic, T. Spatzal, S. L. A. Andrade, O. Einsle, Production and isolation of vanadium nitrogenase from *Azotobacter vinelandii* by molybdenum depletion. *J. Biol. Inorg. Chem.* **22**, 161–168 (2017).

57. W. Kabsch, XDS. *Acta Crystallogr. D Biol. Crystallogr.* **66**, 125–132 (2010).

58. M. D. Winn, C. C. Ballard, K. D. Cowtan, E. J. Dodson, P. Emsley, P. R. Evans, R. M. Keegan, E. B. Krissinel, A. G. W. Leslie, A. McCoy, S. J. McNicholas, G. N. Murshudov, N. S. Pannu, E. A. Potterton, H. R. Powell, R. J. Read, A. Vagin, K. S. Wilson, Overview of the CCP4 suite and current developments. *Acta Crystallogr. D Biol. Crystallogr.* **67**, 235–242 (2011).

59. P. Emsley, B. Lohkamp, W. G. Scott, K. Cowtan, Features and development of *Coot*. *Acta Crystallogr. D Biol. Crystallogr.* **66**, 486–501 (2010).

60. G. N. Murshudov, P. Skubák, A. A. Lebedev, N. S. Pannu, R. A. Steiner, R. A. Nicholls, M. D. Winn, F. Long, A. A. Vagin, REFMAC5 for the refinement of macromolecular crystal structures. *Acta Crystallogr. D Biol. Crystallogr.* **67**, 355–367 (2011).

61. M. Senger, S. Mebs, J. Duan, O. Shulenina, K. Laun, L. Kertess, F. Wittkamp, U. P. Apfel, T. Happe, M. Winkler, M. Haumann, S. T. Stripp, Protonation/reduction dynamics at the [4Fe-4S] cluster of the hydrogen-forming cofactor in [FeFe]-hydrogenases. *Phys. Chem. Chem. Phys.* **20**, 3128–3140 (2018).

62. T. Spatzal, M. Aksoyoglu, L. Zhang, S. L. A. Andrade, E. Schleicher, S. Weber, D. C. Rees, O. Einsle, Evidence for interstitial carbon in nitrogenase FeMo cofactor. *Science* **334**, 940 (2011).

Citation: M. Rohde, K. Laun, I. Zebger, S. T. Stripp, O. Einsle, Two ligand-binding sites in CO-reducing V nitrogenase reveal a general mechanistic principle. *Sci. Adv.* **7**, eabg4474 (2021).

Science Advances

Two ligand-binding sites in CO-reducing V nitrogenase reveal a general mechanistic principle

Michael Rohde, Konstantin Laun, Ingo Zebger, Sven T. Stripp and Oliver Einsle

ARTICLE TOOLS	http://advances.sciencemag.org/content/7/22/eabg4474
SUPPLEMENTARY MATERIALS	http://advances.sciencemag.org/content/suppl/2021/05/24/7.22.eabg4474.DC1
REFERENCES	This article cites 61 articles, 11 of which you can access for free http://advances.sciencemag.org/content/7/22/eabg4474#BIBL
PERMISSIONS	http://www.sciencemag.org/help/reprints-and-permissions

Use of this article is subject to the Terms of Service